ADVANCES IN ATMOSPHERIC SCIENCES, VOL. 34, OCTOBER 2017, 1235–1248

• **Original Paper** •

Variable and Robust East Asian Monsoon Rainfall Response to El Niño over the Past 60 Years (1957–2016)

Bin WANG[1,2], Juan LI[*1,2], and Qiong HE[1]

[1]*Earth System Modeling Center, Nanjing University of Information Science and Technology, Nanjing* 210044*, China*
[2]*Department of Atmospheric Sciences and International Pacific Research Center, University of Hawaii at Manoa, Honolulu Hawaii* 96822*, USA*

(Received 15 Jan 2017; revised 1 Jun 2017; accepted 5 Jun 2017)

ABSTRACT

Severe flooding occurred in southern and northern China during the summer of 2016 when the 2015 super El Niño decayed to a normal condition. However, the mean precipitation during summer (June–July-August) 2016 does not show significant anomalies, suggesting that — over East Asia (EA) — seasonal mean anomalies have limited value in representing hydrological hazards. Scrutinizing season-evolving precipitation anomalies associated with 16 El Niño episodes during 1957–2016 reveals that, over EA, the spatiotemporal patterns among the four categories of El Niño events are quite variable, due to a large range of variability in the intensity and evolution of El Niño events and remarkable subseasonal migration of the rainfall anomalies. The only robust seasonal signal is the dry anomalies over central North China during the El Niño developing summer. Distinguishing strong and weak El Niño impacts is important. Only strong El Niño events can persistently enhance EA subtropical frontal precipitation from the peak season of El Niño to the ensuing summer, by stimulating intense interaction between the anomalous western Pacific anticyclone (WPAC) and underlying dipolar sea surface temperature anomalies in the Indo-Pacific warm pool, thereby maintaining the WPAC and leading to a prolonged El Niño impact on EA. A weak El Niño may also enhance the post-El Niño summer rainfall over EA, but through a different physical process: the WPAC re-emerges as a forced response to the rapid cooling in the eastern Pacific. The results suggest that the skillful prediction of rainfall over continental EA requires the accurate prediction of not only the strength and evolution of El Niño, but also the subseasonal migration of EA rainfall anomalies.

Key words: El Niño impact, monsoon rainfall, East Asian monsoon, Asian monsoon, precipitation variability, monsoon–ocean interaction, western Pacific subtropical high

Citation: Wang, B., J. Li, and Q. He, 2017: Variable and robust East Asian monsoon rainfall response to El Niño over the past 60 years (1957–2016). *Adv. Atmos. Sci.*, **34**(10), 1235–1248, doi: 10.1007/s00376-017-7016-3.

1. Introduction

The 2015/16 El Niño caused widespread hydrological hazards over the Asian monsoon (AM) region. In summer 2015, Northwest India and Indonesia experienced severe drought. From July to October 2015, the amount of precipitation over southern Indonesia reduced to less than 20 mm month^{-1} (about 10% of the climatology). On the other hand, in the summer of 2016, the Yangtze River Valley experienced its worst floods since 1998; widespread floods occurred across the country from southwestern to northern China (http://edition.cnn.com/2016/07/23/asia/china-floods/index.html), causing hundreds of fatalities and huge economic loss.

The AM rainfall anomalies associated with El Niño are strongly season-dependent and evolve most prominently from the El Niño developing summer to decaying summer (Wang et al., 2003; Wu et al., 2003). Figure 1 shows the AM rainfall anomalies associated with the 2015/16 El Niño. The station and satellite records confirm the harshly deficient monsoon rainfall over western India during June–July–August (JJA) 2015, and the extremely deficient rainfall over Indonesia and the Philippines during JJA and September–October–November (SON) 2015. It is notable that the enhanced rainfall occurs along the East Asia (EA) subtropical front continuously from SON 2015 to JJA 2016. Interestingly, the weak seasonal mean anomaly signal in JJA 2016 is not a faithful indicator of the severe flooding situation, suggesting that the seasonal mean anomalies over EA have limited value in representing the hydrological hazard. The reason for this is discussed in section 6.

But is the impact of the 2015/16 El Niño typical compared to other super El Niño episodes? According to the National Oceanic and Atmospheric Administration's Oceanic

* Corresponding author: Juan LI
Email: juanl@hawaii.edu

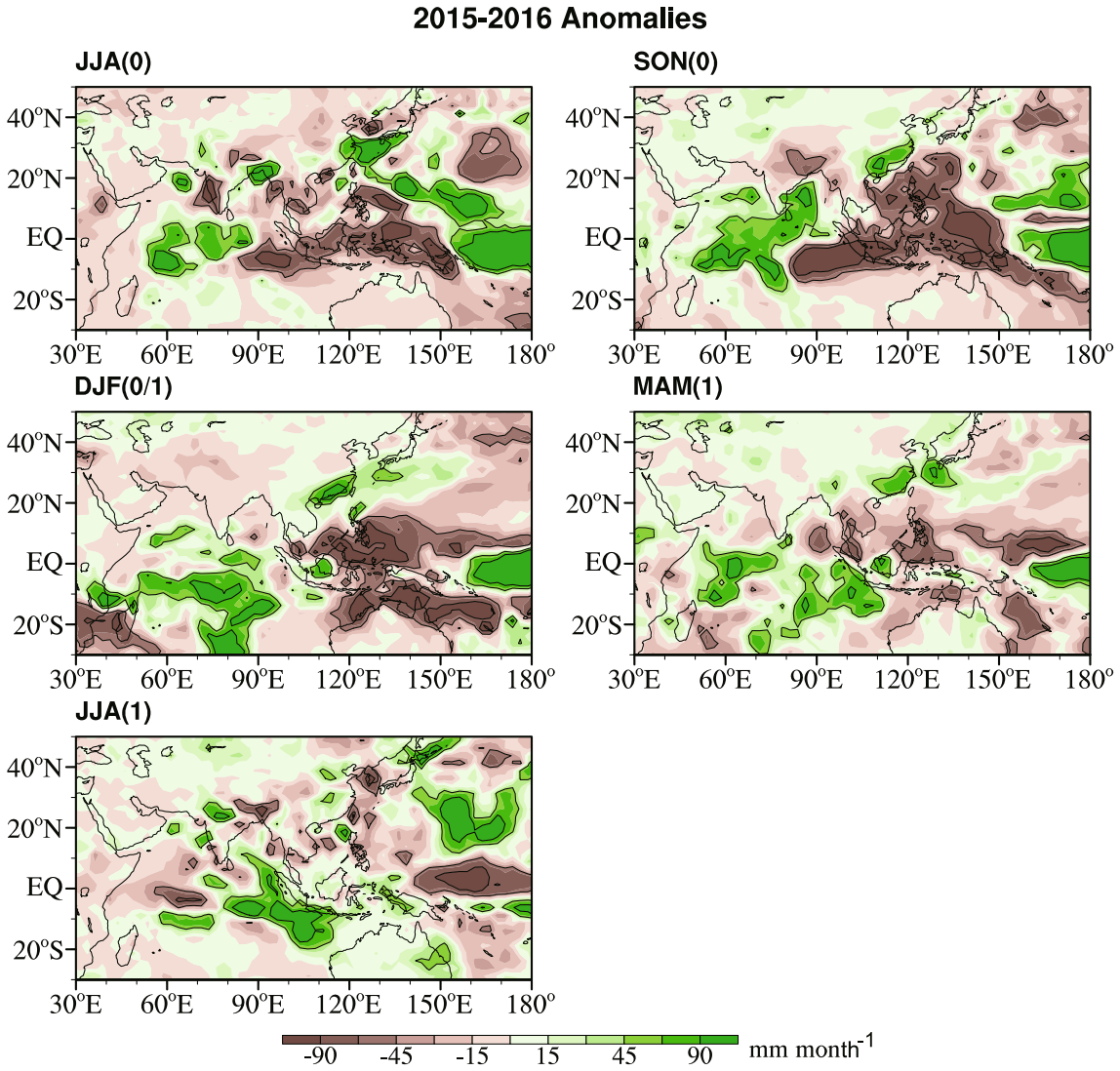

Fig. 1. Seasonal mean precipitation anomalies from JJA 2015 to JJA 2016. Year 0 and year 1 denote the year during which El Niño develops and the following year, respectively. GPCP precipitation data (1979–2016) are used.

Niño Index [ONI — a monthly index defined based on the three-month running mean SST anomalies averaged over the Niño3.4 region (5°N–5°S, 120°–170°W)], a super El Niño can be defined as one in which the ONI is greater than 2°C (http://www.cpc.noaa.gov/products/analysis_monitoring/ensostuff/ensoyears.shtml). Using this criterion, there are three super El Niño events in the last 60 years: 1982/83, 1997/98, and 2015/16 (http://ggweather.com/enso/oni.htm). As shown in Fig. 2, the evolution of monsoon precipitation anomalies for these three super El Niño events is overall similar from JJA(0) to DJF(0/1), but the impacts of the 2015/16 event differ to those of the previous two super El Niño events from MAM(1) to JJA(1), especially over EA. The composite super El Niño anomalies map (Fig. 2d) indicates that the increased rainfall along the EA subtropical front from the developing fall [SON(0)] to MAM(1) is a significant signal, but the composite rainfall anomalies during JJA(1) are generally insignificant.

But how do the impacts of super El Niño on AM rainfall fit in terms of the canonical picture of El Niño impacts? Figure 3 shows a map of the impacts of canonical El Niño on global precipitation, which is taken from the International Research Institute for Climate and Society website, and based on a statistical analysis of historical El Niño events carried out by Ropelewski and Halpert (1987), as well as Mason and Goddard (2001). During an El Niño, the dry anomalies occurring over India, Indonesia, the Philippines and Australia are anticipated from the canonical picture. However, the East Asian monsoon (EAM) rainfall anomalies are absent in the canonical picture. Thus, two questions arise: Should El Niño be blamed for the floods in China in July 2016? And, in general, is there any robust signal of the impact of El Niño on EAM rainfall? The second question is extremely important given that many studies have recognized El Niño and La Niña as major sources of EAM precipitation (e.g., Fu and Li, 1978; Wang and Zhao, 1981; Guo, 1987; Wang and Li, 1990; Zhang

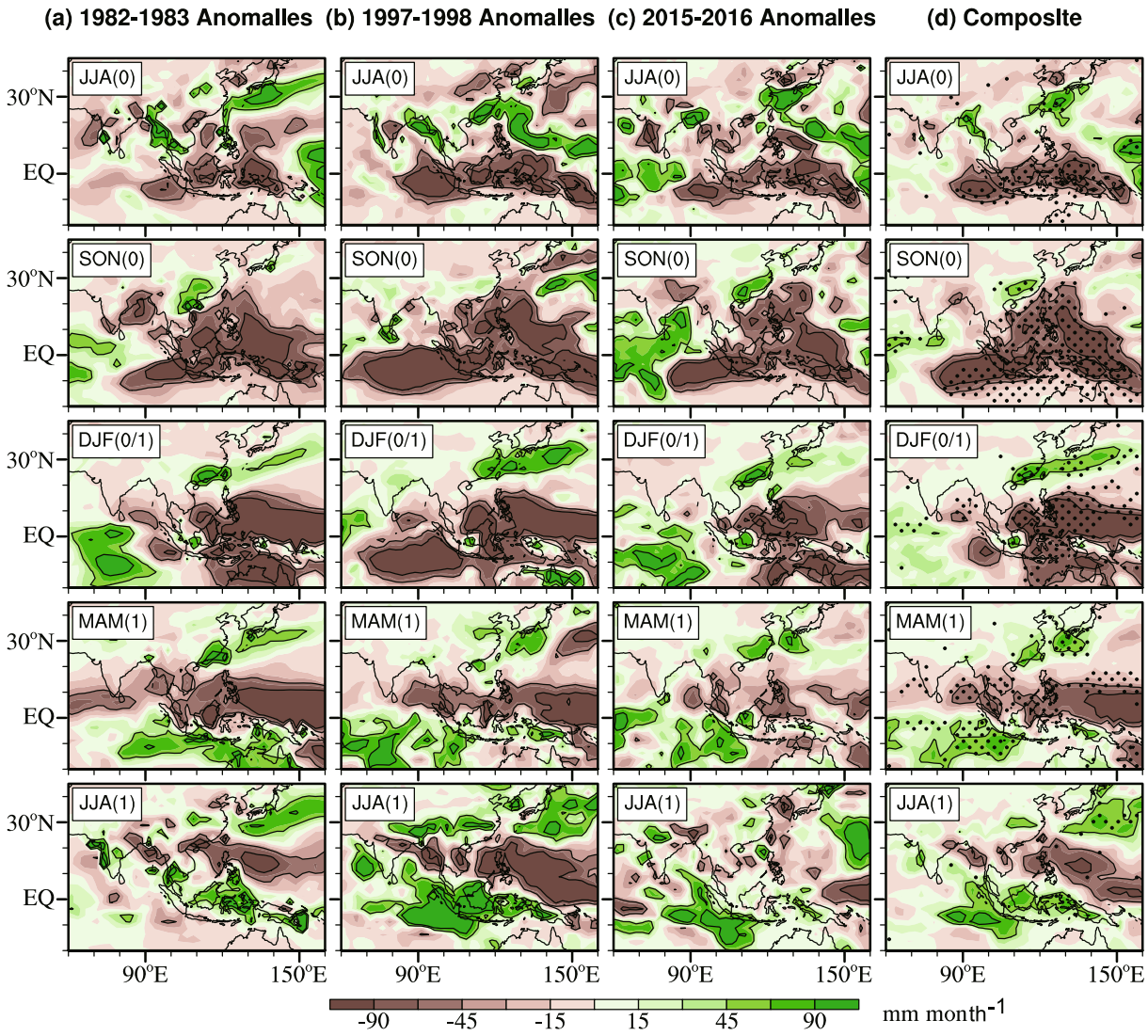

Fig. 2. (a) Seasonal mean precipitation anomalies from JJA 1982 to JJA 1983. (b, c) As in (a), but for 1997/98 and 2015/16, respectively. (d) Composite precipitation anomalies for these three super El Niño events. The dotted area in (d) indicates where the "signal" (composite mean) is greater than the "noise" (2 SD of the composite members). GPCP precipitation data (1979–2016) are used.

et al., 1999; Chang et al., 2000; Wu et al., 2003; Wang et al., 2009a; Yuan and Yang, 2012; Yim et al., 2014a, 2016; Xing et al., 2016).

In this study, we aim to address the above two questions, but we also want to find out (i) under what conditions EA precipitation may have robust responses to El Niño–induced forcing; and (ii) the cause of the variable responses of EAM rainfall to El Niño–induced forcing. Following this introduction, section 2 describes the data used. Section 3 introduces the method for classifying El Niño based on "monsoon-year" intensity. Section 4 synthesizes the variable and robust signals of the EA rainfall response to El Niño. Section 5 discusses why the EA summer rainfall response to El Niño is so variable. In section 6, we address why strong and weak El Niño events impact East Asian summer monsoon (EASM) rainfall differently. The last section (section 7) provides a summary and discusses the implications of our study.

2. Data

The data used in this study comprise the global monthly mean precipitation from version 2.3 of the Global Precipitation Climatology Project (GPCP) dataset (Adler et al., 2003), from January 1979 to August 2016; the monthly mean land precipitation from the Global Precipitation Climatology Centre (GPCC) dataset (Schneider et al., 2014), from January 1957 to August 2016; the monthly mean horizontal wind at 850 hPa from the NCEP–NCAR Reanalysis I dataset (Kalnay et al., 1996), from January 1957 to August 2016; and the monthly sea surface temperature (SST) from the arithmetic mean of two datasets — the Hadley Centre Sea Ice and Sea Surface Temperature (HadISST) dataset (Rayner et al., 2003) and version 4 of the National Oceanic and Atmospheric Administration Extended Reconstructed SST (ERSST) dataset (Huang et al., 2016), from January 1957 to December 2016.

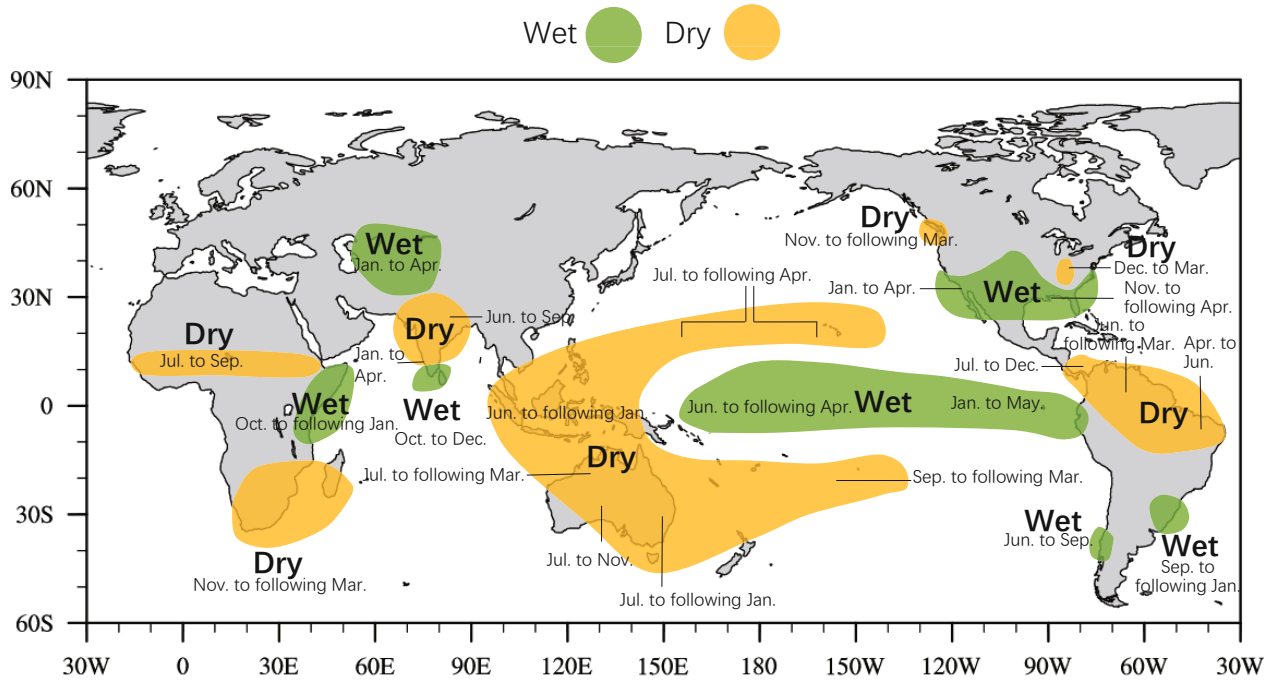

Fig. 3. Canonical picture of the impact of El Niño on global precipitation (adapted from http://iri.columbia.edu/our-expertise/ climate/enso).

In all composite maps, we show the significant signals as those in regions where the composite mean ("signal") is greater than one or two standard deviations (SD) of the spreading member events ("noise").

3. Classification of El Niño events based on "monsoon-year" intensity

To obtain reliable statistics, we examine El Niño–Southern Oscillation (ENSO) during the past 60 years from 1957 to 2016, during which observations of the equatorial Pacific from ship reports are relatively reliable and uniform (Wang, 1995). First, we classify the intensity of El Niño events based on monsoon-year averaged Niño3.4 index (Fig. 4). This index is derived from combined HadISST and ERSST data and normalized over the period 1957–2015. The monsoon year starts from June(0) and ends in May(1), where "0" denotes the El Niño developing year and "1" denotes the decaying year. This definition of the monsoon year is consistent with the concept proposed by Meehl (1987) and Yasunari (1991). More importantly, such a definition of "monsoon year" covers the major phases of development, maturity, and decay, of a typical El Niño event. Therefore, different from the ONI index, the monsoon-year mean Niño3.4 index reflects not only the El Niño maximum intensity but also the integrated intensity during the entire evolution of El Niño, including its development and decay phases. Note also that the monsoon-year ENSO index is a yearly index.

Four categories of El Niño are identified over the past 60 years (Table 1). The criterion of 0.5 SD is commonly adopted

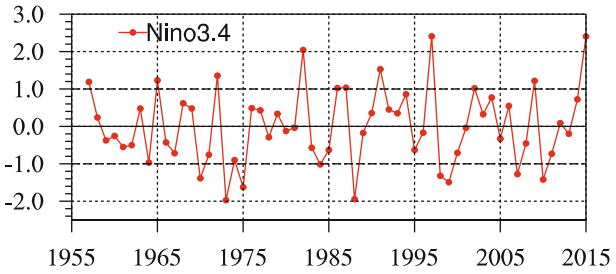

Fig. 4. Time series of normalized Niño3.4 index based on the monsoon year [June(0)–May(1)] during 1957–2015. Combined HadISST and ERSST data are used.

as the definition of an El Niño event, and thus we define a weak El Niño as having an intensity of 0.5–1.0 SD. Similarly, 1 SD is commonly considered as an appropriate threshold for strong anomalies, so we define a strong event as above 1 SD. The separation of minor and moderate events using 0.7 SD is somewhat arbitrary, but results are similar when a value of between 0.7 and 0.8 is used as the demarcation. The resultant classification yields a result that is generally consistent with the classification derived by using the ONI. There are three super El Niño years (> 2 SD) — 1982, 1997 and 2015; five major El Niño years (1–2 SD) — 1957, 1965, 1972, 1991 and 2009; five moderate El Niño years (0.7–1SD) — 1986, 1987, 1994, 2002 and 2004; and five minor El Niño years (0.5–0.7SD) — 1963, 1968, 1969, 1976 and 2006. The super and major El Niños are grouped into the "strong" El Niños, while the minor and moderate El Niños are grouped into the "weak" El Niños.

Figure 5 compares the composite evolution of Niño3.4 index for each category. The years of 1986 and 1987 are outliers due to the odd peak time occurrence in the summer of 1987. For this reason, we remove the 1986 and 1987 events from the moderate event category when composites are made. Both the peak intensity and duration of the positive anomaly (lifespan of an El Niño) gradually reduce from the super to minor El Niño composites. The three super and five major El Niño events show similar evolution. The warming starts early in March–April(0), reaches a peak around November–December, and decays to a normal condition in June(1). In JJA(0), the warming has already reached sizable amplitude (about one-half of the mature phase amplitude). The main difference between the super and major El Niño events is the maximum intensity in their mature phases. Therefore, it is reasonable to combine these two categories to make a single strong El Niño group. For the three moderate and five minor El Niños, their life cycles are short, normally starting from May(0)–June(0) and ending in April(1) or May(1). The Niño3.4 SST anomalies have small spread among the events only from JJA(0) to DJF(0/1). For convenience, we combine the three moderate and five minor events into a single group, named the "weak" El Niño composite.

Table 1. Categories of El Niño events based on their monsoon-year intensity.

Category	Years
Super El Niño (> 2 SD)	1982, 1997, 2015
Major El Niño (1–2 SD)	1957, 1965, 1972, 1991, 2009
Moderate El Niño (0.7–1 SD)	1986, 1987, 1994, 2002, 2004
Minor El Niño (0.5–0.7 SD)	1963, 1968, 1969, 1976, 2006

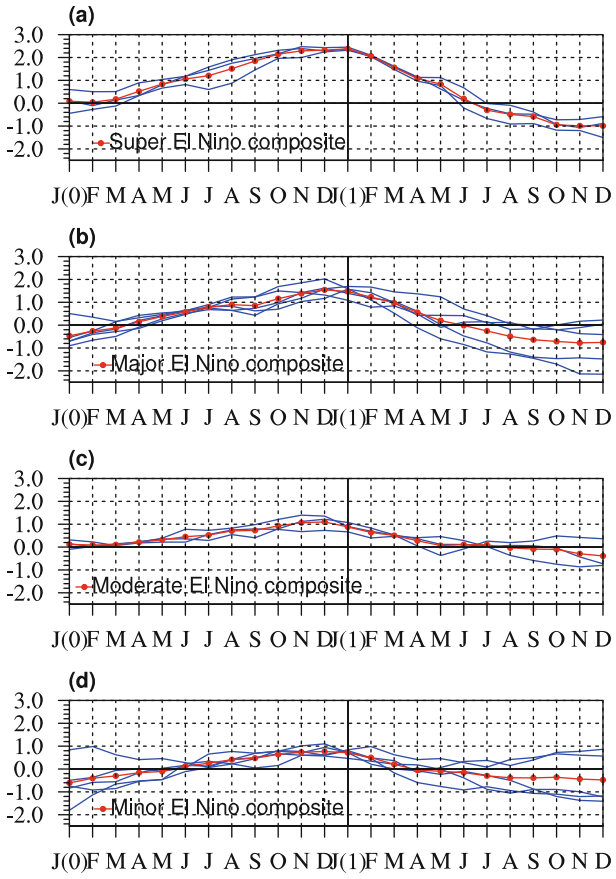

Fig. 5. Composite evolution of Niño3.4 index (red curve) from Jan(0) to Dec(1) for (a) three super, (b) five major, (c) three moderate, and (d) five minor El Niño events. The blue curves indicate the evolution of Niño3.4 index for each individual El Niño event. Combined HadISST and ERSST data are used.

The AM response to ENSO is strongly season-dependent (Wang et al., 2003). Therefore, in the present analysis we present season-dependent, evolving anomalies from the summer of El Niño development (named as Year 0) to the summer of El Niño decay (named as Year 1) or the post-El Niño summer.

4. Variable and robust EA precipitation responses to El Niño forcing

The results in Fig. 2 suggest that the EA region has divergent responses to super El Niño. To scrutinize the variable responses of the EAM precipitation to El Niño forcing, we focus on the EA region and compare the composite maps for the four categories of El Niño events in Fig. 6. Figure 6e shows the composite anomalies for all 16 El Niño events. The red dotted areas indicate the regions where the anomalies in all four categories have the same sign, which helps to identify any robustly common feature. The pink dotted areas denote the regions where three out of four categories have the same sign, which helps to highlight the regions in which anomalies have similar features. The areas with black dots represent two out of four category composites having the same sign, which helps to identify the regions where the rainfall responses are highly variable.

Overall, the variable response is dominant, as evidenced by the large portion of areas with black dots. In particular, during the El Niño decaying summer, the rainfall anomalies show very different patterns among the four-category composites and there is barely a common signal among the four-category composites, making prediction very difficult. If we look at the all-El Niño composites, the signals tend to be dominated by the super El Niño composite. If one takes the all-El Niño composite maps as a guideline for prediction of the El Niño impact, it is important to keep in mind that the precipitation anomalies associated with the different strengths of El Niño can be remarkably variable.

So, among all these variable patterns, are there any robust signals concerning the influence of El Niño on EAM precipitation? Looking for such signals is of critical importance for seasonal prediction. Let us examine the signals that are common or similar to all four-category El Niño events (Fig. 6e). During the El Niño developing summer, the rainfall over central China between the middle reaches of the Yellow River and Yangtze River tends to decrease significantly. During the

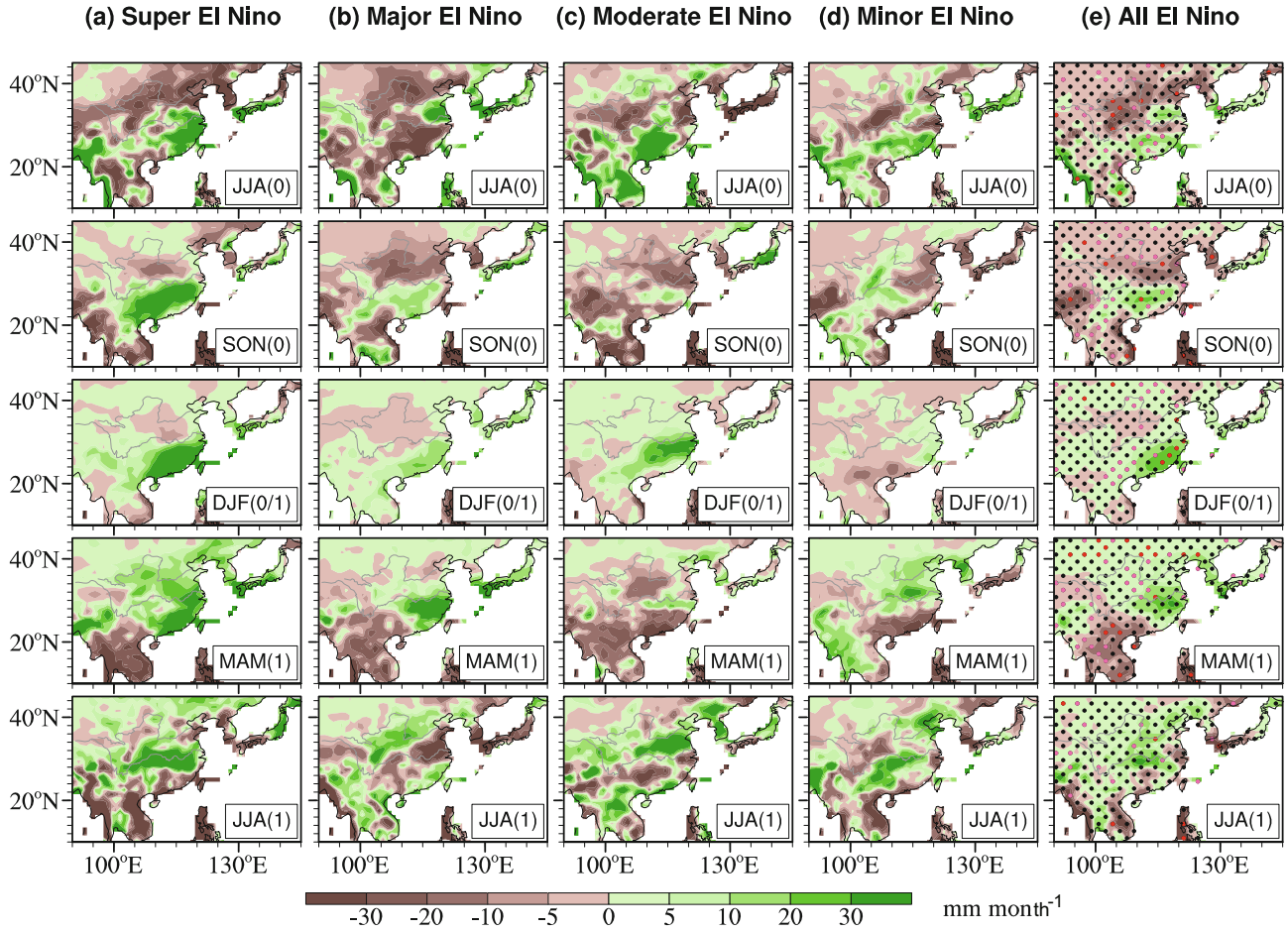

Fig. 6. Composite seasonal mean precipitation anomalies from JJA(0) to JJA(1) for (a) three super, (b) five major, (c) three moderate, (d) five minor, and (e) all 16 El Niño events. In (e), the red, pink and black dotted areas respectively indicate the regions where four out of four, three out of four, and two out of four category composites have the same sign. GPCC data (1957–2016) are used.

winter of the El Niño mature phase, precipitation tends to increase over Zhejiang and Fujian provinces. During MAM(1), dry conditions tend to dominate over Guangxi Province and the western part of the Indochina peninsula.

Figure 6 shows the differences in rainfall anomalies between the strong and weak El Niño events. In Fig. 7, we further compare the season-evolving precipitation anomalies associated with the strong and weak El Niño composites. Here, both the strong and weak group include eight El Niño events.

Figure 7 indicates salient differences in the EAM responses between the strong and weak El Niño cases. The most prominent difference is seen during the three seasons from SON(0) to MAM(1), around the mature phase of El Niño. A strong El Niño induces a robust increase in precipitation over southern China and western Japan, along the EA subtropical frontal zone. However, a weak El Niño event does not cause a consistent anomaly pattern over southern China and western Japan. This suggests that the response of the EA winter monsoon strongly depends on the intensity of El Niño. The large-amplitude anomalies in the strong El Niño composites suggest that EAM precipitation may have a considerably robust signal in response to strong El Niño forcing.

5. Why are the impacts of El Niño on EASM rainfall so variable?

First, the JJA-mean anomalies may not properly reflect the EA rainfall response to El Niño, due to the migratory nature of the rainfall anomalies. This is because EA is a unique subtropical monsoon region between the Eurasian continent and Pacific Ocean. The major rain-producing system over EA is a southwest–northeast oriented subtropical front — a convergent zone between the moist southwesterlies associated with the western Pacific subtropical high (WPSH) and dry air advected from the north. Climatologically, the frontal zone migrates from South China in June to North China in August. As shown in Fig. 8, during the El Niño decaying summer from June to August, the rainfall anomalies also migrate northwards, following the climatological northward migration of the subtropical front. Due to the concentration of rainfall in the narrow EA subtropical frontal zone, as well as the continuous northward migration of the subtropical front, heavy rainfall normally occurs during a relatively short rainy period; therefore, the rainfall anomalies vary remarkably from month to month. This is partly why the EA precipitation response to El Niño is so variable in terms of

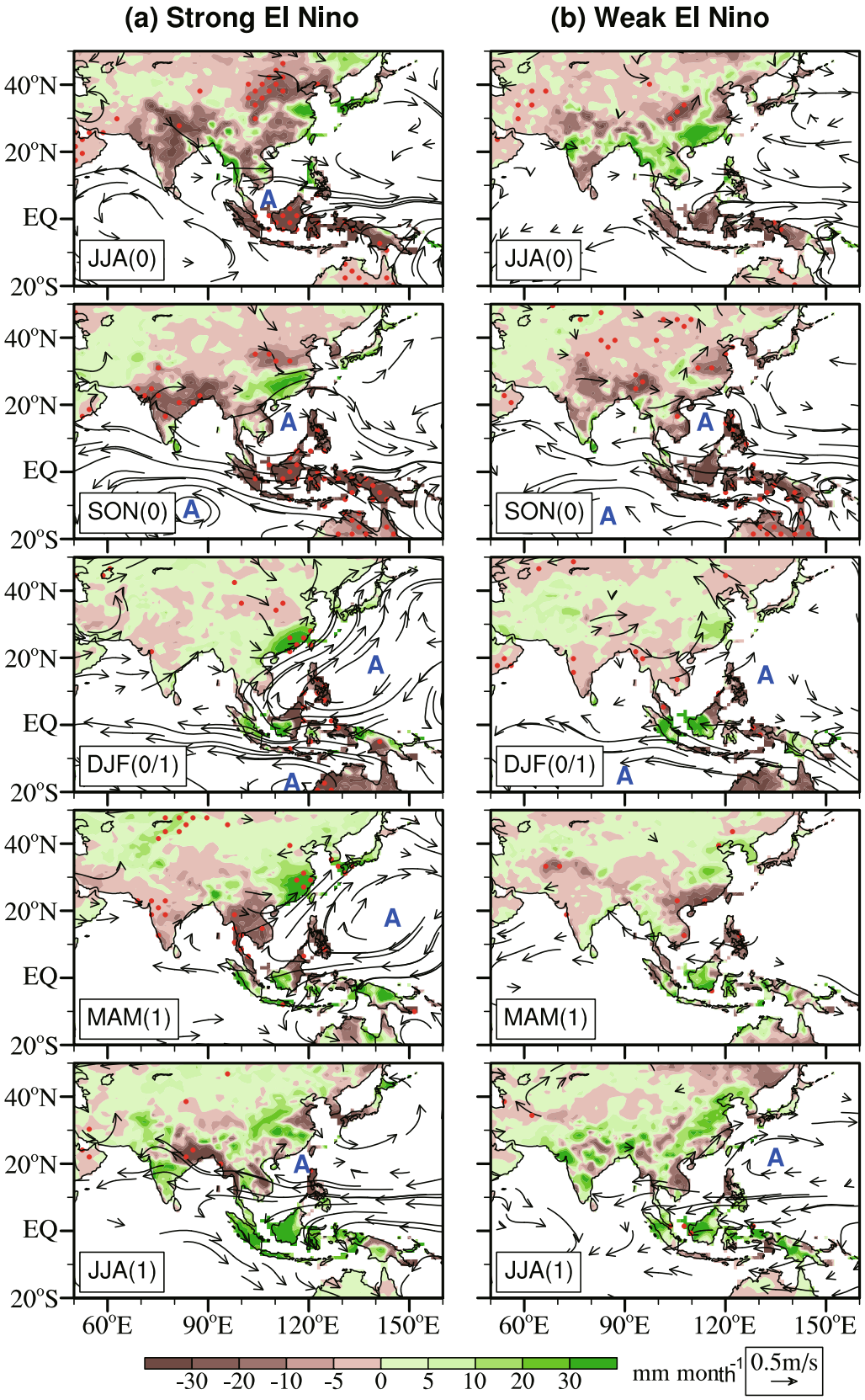

Fig. 7. Composite seasonal mean precipitation and 850-hPa wind anomalies for (a) the eight strong (1957, 1965, 1972, 1982, 1991, 1997, 2009 and 2015) and (b) eight weak (1963, 1968, 1969, 1976, 1994, 2002, 2004 and 2006) El Niño events. The dotted areas indicate where the "signal" (composite mean) is greater than the "noise" (1 SD of the composite members). The "A" in blue indicates the anticyclonic circulation. GPCC precipitation data and NCEP–NCAR reanalysis I data for 1957–2016 are used.

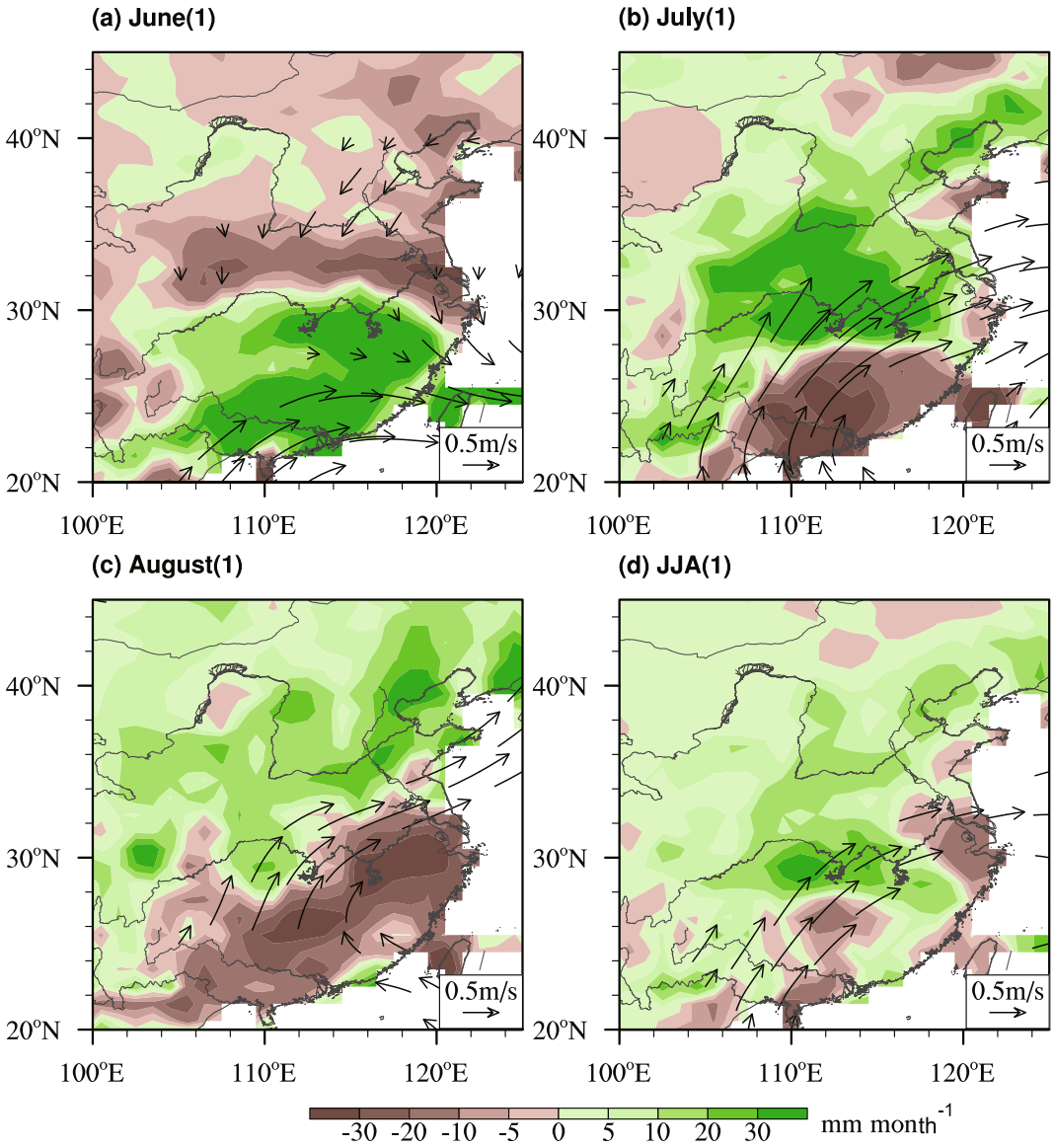

Fig. 8. All-El Niño (16 events) composite precipitation and 850-hPa wind anomalies for (a) June(1), (b) July(1), (c) August(1), and (d) JJA(1). GPCC precipitation data and NCEP–NCAR reanalysis I data for 1957–2016 are used.

geographic location and time of occurrence. This is also the reason why floods occurred from southern to northern China in summer 2016, despite the weak seasonal mean anomaly. Over EA, the JJA precipitation anomaly may not necessarily reflect flooding events well. It has been shown that ENSO affects the EA early summer (May–June) and peak summer (July–August) mean rainfall anomalies differently (Wang et al., 2009a, Yim et al., 2016, Xing et al., 2016, 2017).

Second, the diversity of El Niño, such as its different intensities and evolutions (Fig. 5), can also cause variable responses of the EA summer rainfall. Different locations of maximum SST anomalies have been shown to have different impacts on the EAM (Yuan and Yang, 2012). Since the central Pacific El Niño falls into the weak category, the impacts of the maximum-SST location are reflected in the differences between the strong and weak El Niño events. As seen from Fig. 5, the strength of El Niño tends to have larger spread during the post-El Niño summer compared to the developing summer. This explains why the rainfall response during the El Niño decaying summer is more variable than during its developing phase.

Third, but not least importantly, the EASM is an indirect response to El Niño forcing during both the developing summer and decaying summer. During the decaying summer, the EA subtropical front zone is sensitively dependent on the strength and location of the WPSH, which is largely determined by the local atmosphere–ocean interaction rather than the El Niño forcing, as discussed in detail in the next section. The WPSH also varies strongly on the intraseasonal time scale during summer (Wang and Zhang, 2002), adding additional uncertainties.

During the El Niño developing summer, the eastern and

central Pacific warming has already reached one-half of its maximum intensity (Fig. 5). This warming strength is sufficient to alter the tropical circulation and Indian monsoon. The most robust feature common to both the strong and weak El Niño cases is seen over the Maritime Continent (MC), where the composite rainfall anomalies for strong and weak El Niños show a remarkably similar evolution from JJA(0) to JJA(1) (Fig. 7). Another relatively robust response to the El Niño forcing is seen over India during JJA(0) and SON(0). Central North China tends to have reduced rainfall, but the intensity and locations of this reduction in rainfall are quite different in strong and weak events. This makes the EAM response to El Niño forcing less robust than that of the Indian summer monsoon.

Figure 9 illustrates the process by which a developing El Niño affects AM rainfall. The question arises: why does El Niño have the most robust impacts over the MC? The equatorial waveguide is the most effective teleconnection bridge in which the equatorial Kelvin and Rossby waves act as efficient agents to adjust atmospheric circulation anomalies. This process is responsible for the zonal shift of the Walker cell. So, MC rainfall directly responds to changes in eastern Pacific SST, resulting in the most robust reduction of rainfall during El Niño developing summer.

Also, why is the Indian monsoon response less robust than that of the MC? First, the Indian monsoon response is an indirect response. It is the reduced precipitation heating over the MC that further excites descending Rossby waves to its west and north, forming an elongated anticyclonic ridge extending from the MC to India, thereby causing deficient Indian summer rainfall (Fig. 7). This Rossby wave response is enhanced by the presence of an easterly vertical shear of the mean monsoon circulation (Wang et al., 2003). Second, the monsoon–ocean interaction over the Indian Ocean tends to offset the remote impacts of ENSO by inducing the Indian Ocean Dipole (IOD, or zonal) mode (Saji et al., 1999; Webster et al., 1999; Li et al., 2003; Wang et al., 2003) and/or by directly warming the northern Indian Ocean (Lau and Nath, 2000). The 1997 El Niño is an example: the increased rainfall over India caused by the El Niño-induced IOD offsets the El Niño-induced drought, thus resulting in a normal monsoon.

Further still, why does central North China respond to the El Niño forcing less robustly than the Indian summer monsoon? The rainfall anomalies over central North China tend to correlate positively with those over northern India during the El Niño developing summer [see the review by Wu (2017)]. The impact of El Niño on the rainfall over central North China primarily takes place through its impact on the Indian monsoon. When the Indian monsoon is weak, the reduced precipitation heating over India generates an anomalous low pressure in the upper troposphere over central Asia through an atmospheric Rossby wave response. The central Asian low further excites a barotropic Rossby wave train along the waveguide provided by the westerly jet stream. This wave train travels all the way to the North Pacific and North Atlantic — a pattern called the circumglobal teleconnection (CGT) (Ding and Wang, 2005). One of the anomalous lows on this CGT wave train weakens the northern part of the WPSH, reducing the moisture transport to northern China and decreasing the rainfall over that region. This part of the CGT from central Asia to the western Pacific is also named the "Silk Road teleconnection" (Enomoto et al., 2003). For a more detailed discussion of the mechanisms involved, readers are referred to Ding et al. (2011) and Wu (2017).

6. Why strong and weak El Niño cases affect EA summer rainfall differently

6.1. *Why does enhanced precipitation over southern China occur only during strong El Niño events?*

To address this question, we examine the low-level (850-hPa) circulation anomalies associated with the evolution of El Niño (Fig. 7). During the strong El Niño events, the enhanced precipitation over southern China and along the EA subtropical front zone from SON(0) to MAM(1) is caused by the anomalous warm and moist southwest flows in the northwest flank of the western Pacific anticyclone (WPAC) anomaly. The WPAC anomaly occurs during SON(0) near the northern Philippines, further develops and expands eastwards during DJF(0/1) and MAM(1), and weakens but maintains to JJA(1). This evolution confirms the previous findings of Wang and Zhang (2002). Clearly, a persistent WPAC anomaly is the circulation system responsible for a wet southern China from SON(0) to MAM(1), and a dry Indochina during MAM(1).

In contrast, during the weak El Niño events, the anoma-

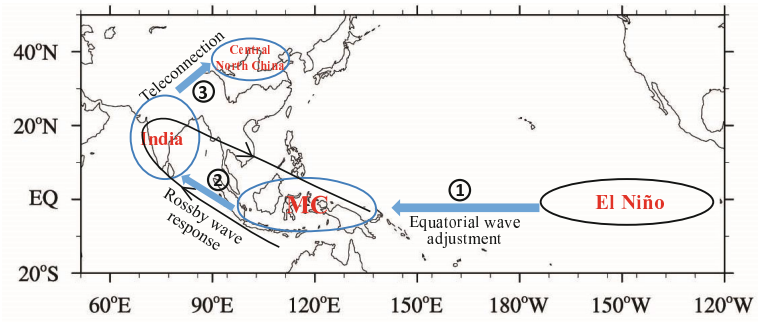

Fig. 9. Schematic diagram showing the process by which a developing El Niño affects Asian summer monsoon rainfall.

lous anticyclone occurs over the South China Sea during SON(0), but then weakens significantly and moves eastwards over the Philippine Sea during DJF(0/1), before finally disappearing in MAM(1). As such, the WPAC only marginally affects the winter precipitation over the EA subtropical front and exerts no significant impact on southern China and Japan in MAM(1). The difference in the strength of the WPAC was noticed in the early work of Wang et al. (2000), who pointed out that the intensity of the WPAC increases with increasing ENSO intensity. They carried out a composite analysis of only six strong El Niño events. During weak El Niño events, the intensity of El Niño during SON(0) is weak, and the excited WPAC anomaly over the South China Sea is also weak (Fig. 7b). As a result, the weak atmosphere–ocean interaction cannot overcome other damping effects, such that the WPAC anomaly decays rapidly.

6.2. *Why only strong El Niño events have a prolonged enhancement of EA subtropical frontal precipitation*

Inspection of the SST anomalies associated with the WPAC can provide a clue (Fig. 10). During the strong El Niño events, the WPAC is coupled with a pronounced anomalous SST dipole: a cooling to its east and southeast (ESE) in the western North Pacific (WNP), and a warming to its west and northwest (WNW) over the EA marginal seas and the northern Indian Ocean (NIO) from the El Niño developing fall to the decaying summer (Fig. 10a). This coupling provides a positive thermodynamic feedback between the WPAC and underlying SST dipole anomaly in the Indo-Pacific warm pool, which amplifies the WPAC from fall to spring, and maintains it to the El Niño decaying summer (Wang et al., 2000; Lau et al., 2004). The mechanism that maintains the WPAC anomaly is summarized in Fig. 11.

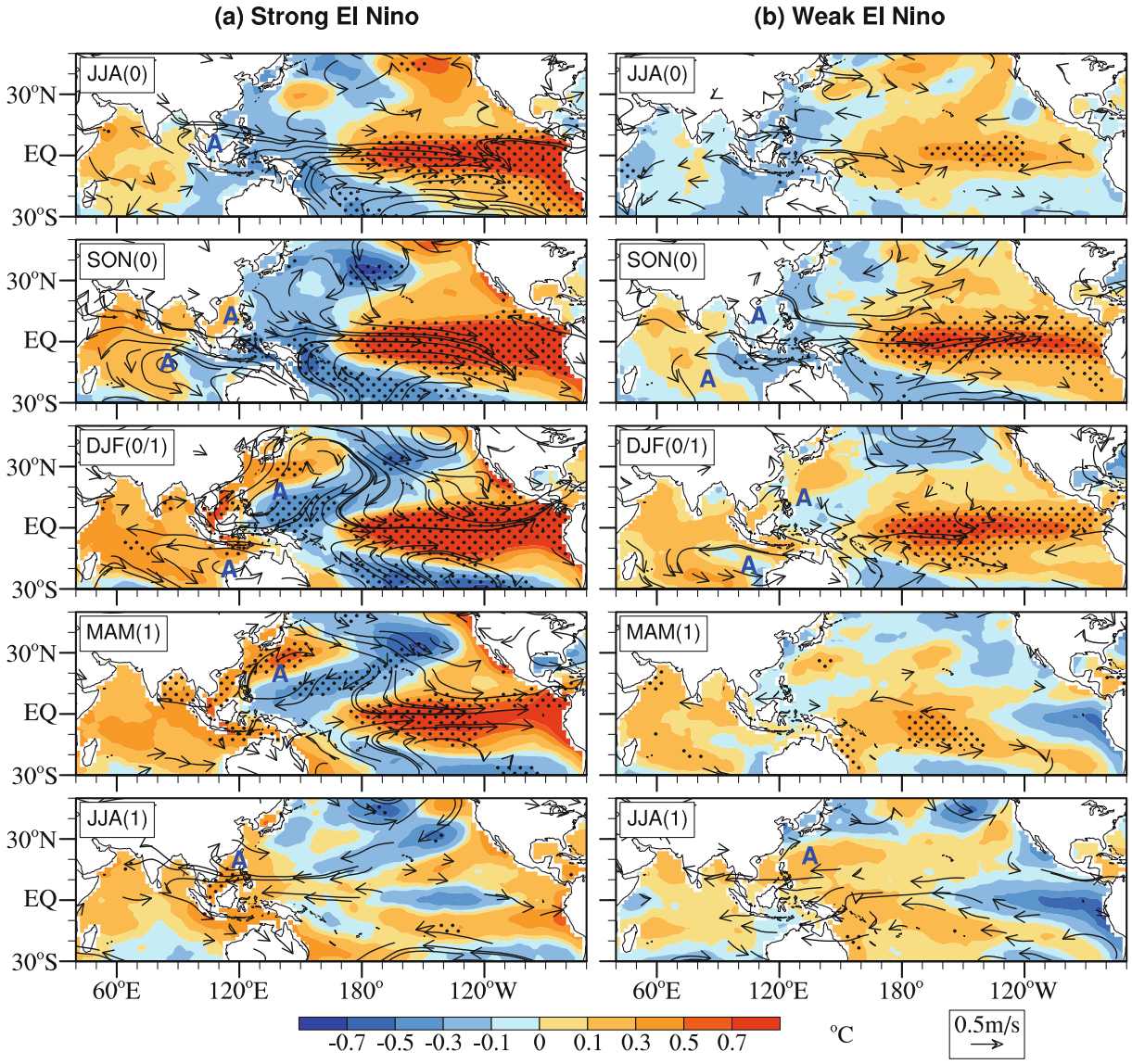

Fig. 10. As in Fig. 7, except for the composite SST and 850-hPa wind anomalies. NCEP–NCAR reanalysis I data, as well as combined HadISST and ERSST data, are used.

First, to the ESE of the WPAC anomaly, the SST is cooled by the anomalous northeasterly winds, because the anomalous northeasterly winds strengthen the mean northeasterlies, thereby enhancing evaporation and entrainment cooling. This *in situ* cooling can suppress deep convection on the ESE side of the WPAC. Conversely, the reduced convective heating generates descending, westward—propagating atmospheric Rossby waves that reinforce the WPAC anomaly in their westward, decaying journey (Wang et al., 2000). This positive thermodynamic feedback between the WPAC and underlying warm pool dipole SST anomaly has been demonstrated by numerical experiments with coupled atmosphere–ocean models, which show that the air–sea interaction can amplify and maintain the WPAC from winter to early summer (Lau and Nath, 2003; Lau et al., 2004; Lau and Wang, 2006; Chowdary et al., 2010).

Second, over the NIO, the ridge of the WPAC extends westwards to the Bay of Bengal, such that the associated anomalous subsidence and easterlies penetrate the NIO (Fig. 10a), increasing downward solar radiation flux and reducing evaporation cooling, thus warming the NIO (Du et al., 2009). In turn, the NIO warming will tend to increase precipitation heating, which excites an easterly equatorial Kelvin wave over the far western Pacific, and the associated anticyclonic shear vorticity can enhance the anomalous WPAC — a process vibrantly coined the "Indian Ocean capacitor" mechanism (Xie et al., 2009, 2016).

The delayed occurrence of the basin-wide warming over the Indian Ocean is a result of the atmosphere–ocean interaction induced by the remote forcing from the eastern-central Pacific through atmospheric teleconnection (Yang et al., 2007). One should consider this delayed Indian Ocean warming effect in terms of coupled atmosphere–ocean dynamics, rather than treating the Indian Ocean warming as a forcing of the atmosphere, as is wrongly the case in some AMIP-type experiments. The notion of treating the monsoon and warm ocean as a coupled system has been elaborated in many previous studies (Webster et al., 1999; Lau and Nath, 2000; Wang et al., 2003). It is recognized that AMIP-type experiments cannot simulate monsoon anomalies, even given the strongest El Niño forcing of 1997/98 (Wang et al., 2004). Over the precipitating summer monsoon regions, the SST is generally a passive response to the atmosphere, rather than a forcing (Wang et al., 2005). Therefore, the effect of the Indian Ocean warming should be demonstrated by numerical experiments with coupled models (Lau et al., 2005; Chowdary et al., 2010; Wang et al., 2013; Xiang et al., 2013).

Note that the role of the Indian Ocean warming and the processes by which Indian Ocean warming affects the WPAC anomaly remain under debate. Wu et al. (2009) argued that the forcing of the Indian Ocean warming on the WPAC is only evident in late boreal summer, when the western Pacific monsoon trough is established; and it is the SST cooling in the western Pacific that drives the WPAC in the early summer before the establishment of the western Pacific monsoon trough. On the other hand, Xiang et al. (2013) showed that local convection–wind–evaporation–SST (CWES) feedback can maintain an anomalous WPAC from May into August, although the negative SST anomaly to the ESE of the WPAC has a small amplitude of a few tenths of a degree. The reason is that the CWES mechanism relies on summer mean flows and precipitation; in the late summer, the enhanced mean precipitation associated with the strong WNP monsoon trough and the high background SST make the atmospheric response to a local SST cooling much more sensitive than in the early summer. In addition, we propose two new mechanisms that may contribute to the maintenance and enhancement of the WPAC during July–August of the post-El Niño summer, which have not been well recognized in the literature. First, during the July–August of post-El Niño summer, the eastern-central Pacific often experiences a rapid transition from a strong warming to a weak cooling. The remote forcing from such a development of La Niña in the central-eastern Pacific can significantly enhance the WPAC anomaly. Second, the northerly wind anomalies to the east of the WPAC can advect dry air from the north to the ESE side of the WPAC, reducing the moisture supply and convective instability, thereby suppressing convection on the ESE side of the WPAC, even

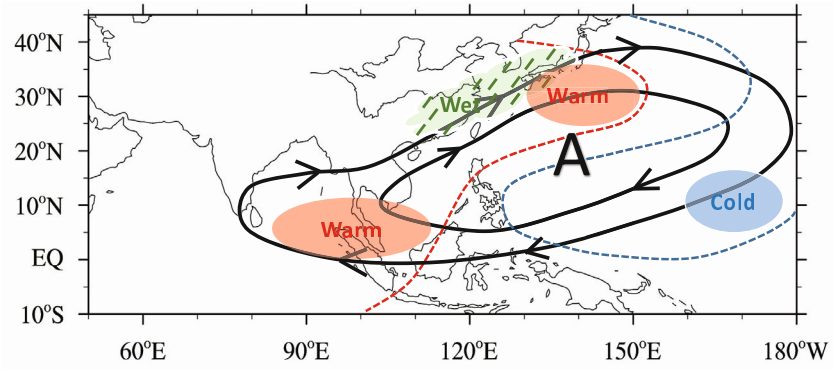

Fig. 11. Schematic diagram showing the interaction between the WPSH and Indo-Pacific SST dipole. This figure is drawn based on the composite anomalies during the MAM(1) season associated with strong El Niño events shown in Figs. 7a and 10a. The "A" in black indicates the anticyclonic circulation.

though the in-situ sea surface cooling is weak or absent.

6.3. *Why weak El Niño events sometimes also enhance rainfall over the Yangtze River Valley and northern China during the post-El Niño summer*

Figure 7 shows that the increased rainfall in both the strong and weak El Niño composites is associated with a WPAC anomaly. However, the origins of the WPAC are different. In the strong El Niño composite, the WPAC is a continuation from winter to summer primarily due to the interaction of the WPAC and the Indo-Pacific warm pool SST dipole, which is evident from SON(0) to JJA(1) (Fig. 10a). Therefore, the strong El Niño impacts can be significantly amplified and prolonged by monsoon–ocean interaction over the Indo-Pacific warm pool, affecting the EASM and WNP tropical storms during the decaying phase of strong El Niño events. In contrast, during the weak El Niño events, the eastern Pacific warming ends earlier in the spring [MAM(1)], so that the WPAC is absent (Fig. 10b). By JJA(1), however, the eastern Pacific SST evolves into a cold phase and the WPAC re-emerges during the summer JJA(1) as a forced response to the eastern Pacific cooling. This can be seen from Fig. 10b: the easterly anomalies generated by the east–west equatorial SST gradients prevail across the entire Pacific and the shear vorticity associated with the easterly anomalies generates the anomalous WPAC.

7. Summary

In the canonical picture of El Niño impacts on global precipitation, EA is a blank area without any signal of impact (Fig. 3). On the other hand, conspicuous precipitation anomalies occurred during the 2015/16 El Niño over EA; and in particular, severe hydrological hazards occurred during the summer of 2016. To comprehend this quandary, we compare the impacts of the 2015/16 super El Niño with the 15 other El Niño episodes that have occurred over the past 60 years. The major findings of this study are as follows:

(1) Severe flood hazards occurred over southern and northern China during the summer of 2016 when the super El Niño at that time decayed to a normal condition. However, the mean precipitation during summer (JJA) 2016 does not show significant anomalies, suggesting that the seasonal mean anomalies over EA have limited value in representing hydrological hazards. While the increased rainfall along the EA subtropical front from the El Niño developing fall to the ensuing spring is a common signal of the impacts of the three super El Niño events, the JJA rainfall anomaly in the post-super El Niño summer is quite variable, and no significant common signal is found.

(2) The season-evolving precipitation anomalies associated with the 16 El Niño episodes show that, over EA, the spatiotemporal patterns among the four categories of El Niño events are primarily variable (Fig. 6). The only robust seasonal signals are the dry anomaly over central North China during the El Niño developing summer, and some locally enhanced rainfall over the southeast coast of China during the El Niño mature phase.

(3) There are generally quite notable differences between the strong and weak El Niño composites (Fig. 7). The most prominent difference is seen during the three seasons from SON(0) to MAM(1) along the EA subtropical frontal zone. Only strong El Niño events can persistently enhance EA subtropical frontal precipitation from the peak season of El Niño to the ensuing summer, by stimulating intense interaction between the anomalous WPAC and underlying dipolar SST anomalies in the Indo-Pacific warm pool, thereby maintaining the WPAC and leading to a prolonged El Niño impact on EA. A weak El Niño may also enhance the post-El Niño summer rainfall over EA, but through a different physical process: the WPAC re-emerges as a forced response to the rapid cooling in the eastern Pacific.

We attribute the variable and uncertain responses of EA summer rainfall to three main sources. First, the JJA mean anomalies may not properly reflect the EA rainfall response to El Niño, due to remarkable subseasonal migration of the rainfall anomalies. The EA rainfall anomalies associated with El Niño migrate northwards from May to August, so the JJA mean can substantially underestimate the amplitude of the rainfall anomalies in each individual month. Second, the diversity of El Niño, such as its different intensities and evolutions (Fig. 5), can cause uncertainties in the responses of EA summer rainfall, especially during the post-El Niño summer when eastern central Pacific SST has a large range of variability. Third, the EASM is only indirectly affected by El Niño. A developing El Niño reduces rainfall over central North China, primarily through a teleconnection from reduced ISM rainfall. The ISM response to El Niño is less robust than over the MC, due to atmosphere–ocean interaction over the Indian Ocean. The teleconnection is further affected by the ISM anomaly and the summer mean state, adding additional uncertainty.

To date, the summer monsoon seasonal precipitation over land and outside the deep tropics has remained a major challenge in climate science, especially over EA (Wang et al., 2009b). Over EA, the diverse spatiotemporal structures of the EAM responses to El Niño pose a great challenge for dynamic models in predicting summer rainfall. The divergent responses are partially due to the different intensities and evolutions of El Niño; but more importantly, it is due to the remarkable northward migration of the EA rainfall anomalies from June to August, which can obscure the El Niño–induced JJA mean anomalies. Thus, prediction of the JJA mean anomaly has limited value in representing hydrological hazards. This explains why a robust EA rainfall response to El Niño has not been fully recognized in the literature outside the EAM community (Fig. 3). The divergent responses may also explain why current dynamical models possess very limited skill in their forecasting of summer mean precipitation.

The results of our study suggest that, in order to skillfully forecast rainfall over continental EA, dynamical models must be able to accurately predict not only the strength, location and evolution of El Niño, but also the subseasonal migration of the subtropical EAM rain bands. In addition, the tra-

ditional method of predicting JJA mean precipitation anomalies needs to change. Prediction of the May–June mean and July–August mean might be more fruitful, as demonstrated in recent predictability studies of the early and late summer EA rainfall anomaly patterns using physics-based empirical models (Wang et al., 2009a, Yim et al., 2014b, 2016; Xing et al., 2016, 2017).

Acknowledgements. This study was supported by the National Natural Science Foundation of China (Grant No. 41420104002) and the National Research Foundation of Korea through a Global Research Laboratory grant of the Korean Ministry of Education, Science and Technology (Grant No. 2011-0021927) and the Atmosphere–Ocean Research Center (AORC). The AORC is partially funded by Nanjing University of Information Science and Technology (NUIST). This paper is NUIST-Earth System Modeling Center publication number 163, School of Ocean and Earth Science and Technology publication number 10027, and International Pacific Research Center publication number 1259.

REFERENCES

Adler, R. F., and Coauthors, 2003: The version-2 global precipitation climatology project (GPCP) monthly precipitation analysis (1979-Present). *Journal of Hydrometeorology*, **4**, 1147–1167, doi: 10.1175/1525-7541(2003)004<1147:TVGPCP>2.0.CO;2.

Chang, C.-P., Y. S. Zhang, and T. Li, 2000: Interannual and interdecadal variations of the east Asian summer monsoon and tropical Pacific SSTs. Part I: Roles of the Subtropical Ridge. *J. Climate*, **13**, 4310–4325, doi: 10.1175/1520-0442(2000)013<4310:IAIVOT>2.0.CO;2.

Chowdary, J., S.-P. Xie, J.-Y. Lee, Y. Kosaka, and B. Wang, 2010: Predictability of summer northwest Pacific climate in 11 coupled model hindcasts: Local and remote forcing. *J. Geophys. Res.*, **115**, D22121, doi: 10.1029/2010JD014595.

Ding, Q. H., and B. Wang, 2005: Circumglobal teleconnection in the northern hemisphere summer. *J. Climate*, **18**, 3483–3505, doi: 10.1175/JCLI3473.1.

Ding, Q. H., B. Wang, J. M. Wallace, and G. Branstator, 2011: Tropical-extratropical teleconnections in boreal summer: Observed interannual variability. *J. Climate*, **24**, 1878–1896, doi: 10.1175/2011JCLI3621.1.

Du, Y., S.-P. Xie, G. Huang, and K. M. Hu, 2009: Role of air-sea interaction in the long persistence of EL Niño-induced north Indian Ocean Warming. *J. Climate*, **22**, 2023–2038, doi: 10.1175/2008JCLI2590.1.

Enomoto, T., B. J. Hoskins, and Y. Matsuda, 2003: The formation mechanism of the Bonin high in August. *Quart. J. Roy. Meteor. Soc.*, **129**, 157–178, doi: 10.1256/qj.01.211

Fu, C., and K. R. Li, 1978: The effects of tropical ocean on the western Pacific subtropical high. *Oceanic Selections*, No. 2, Ocean Press, 16–21.

Guo, Q. Y., 1987: The east Asia monsoon and the Southern Oscillation, 1871–1980. *The Climate of China and Global Climate*, D.-Z. Ye et al., Eds., Spinger-Verlag, 249–255.

Huang, B. Y., and Coauthors, 2016: Further exploring and quantifying uncertainties for extended reconstructed sea surface temperature (ERSST) version 4 (v4). *J. Climate*, **29**, 3119–3142, doi: 10.1175/JCLI-D-15-0430.1.

Kalnay, E., and Coauthors, 1996: The NCEP/NCAR 40-year reanalysis project. *Bull. Amer. Meteor. Soc.*, **77**, 437–471, doi: 10.1175/1520-0477(1996)077<0437:TNYRP>2.0.CO;2.

Lau, N.-C., and M. J. Nath, 2000: Impact of ENSO on the variability of the Asian-Australian monsoons as simulated in GCM experiments. *J. Climate*, **13**, 4287–4309, doi: 10.1175/1520-0442(2000)013<4287:IOEOTV>2.0.CO;2.

Lau, N.-C., and M. J. Nath, 2003: Atmosphere-ocean variations in the Indo-Pacific sector during ENSO episodes. *J. Climate*, **16**, 3–20, doi: 10.1175/1520-0442(2003)016<0003:AOVITI>2.0.CO;2.

Lau, N.-C., and B. Wang, 2006: Interactions between the Asian monsoon and the El Niño/Southern Oscillation. *The Asian Monsoon*, B. Wang, Ed., Springer, Berlin Heidelberg, 479–512, doi: 10.1007/3-540-37722-0_12.

Lau, N.-C., M. J. Nath, and H. L. Wang, 2004: Simulations by a GFDL-GCM of ENSO related variability of the coupled atmosphere-ocean system in the East Asia monsoon region. *East Asian Monsoon*, C. P. Chang, Ed., World Scientific, 271–300, doi: 10.1142/9789812701411_0007.

Lau, N.-C., A. Leetmaa, M. J. Nath, and H.-L. Wang, 2005: Influences of ENSO-induced Indo-Western Pacific SST anomalies on extratropical atmospheric variability during the Boreal summer. *J. Climate*, **18**, 2922–2942, doi: 10.1175/JCLI3445.1.

Li, T., B. Wang, C.-P. Chang, and Y. S. Zhang, 2003: A theory for the Indian Ocean dipole-zonal mode. *J. Atmos. Sci.*, **60**, 2119–2135, doi: 10.1175/1520-0469(2003)060<2119:ATFTIO>2.0.CO;2.

Mason, S. J., and L. Goddard, 2001: Probabilistic precipitation anomalies associated with ENSO. *Bull. Amer. Meteor. Soc.*, **82**, 619–638, doi: 10.1175/1520-0477(2001)082<0619:PPAAWE>2.3.CO;2.

Meehl, G. A., 1987: The annual cycle and interannual variability in the Tropical Pacific and Indian Ocean regions. *Mon. Wea. Rev.*, **115**, 27–50, doi: 10.1175/1520-0493(1987)115<0027:TACAIV>2.0.CO;2.

Rayner, N. A., D. E. Parker, E. B. Horton, C. K. Folland, L. V. Alexander, D. P. Rowell, E. C. Kent, and A. Kaplan, 2003: Global analyses of sea surface temperature, sea ice, and night marine air temperature since the late nineteenth century. *J. Geophys. Res.*, **108**, 4407, doi: 10.1029/2002JD002670.

Ropelewski, C. F., and M. S. Halpert, 1987: Global and regional scale precipitation patterns associated with the El Niño/southern oscillation. *Mon. Wea. Rev.*, **115**, 1606–1626, doi: 10.1175/1520-0493(1987)115<1606:GARSPP>2.0.CO;2.

Saji, N. H., B. N. Goswami, P. N. Vinayachandran, and T. Yamagata, 1999: A dipole mode in the tropical Indian Ocean. *Nature*, **401**, 360–363.

Schneider, U., A. Becker, P. Finger, A. Meyer-Christoffer, M. Ziese, and B. Rudolf, 2014: GPCC's new land surface precipitation climatology based on quality-controlled in situ data and its role in quantifying the global water cycle. *Theor. Appl. Climatol.*, **115**, 15–40, doi: 10.1007/s00704-013-0860-x.

Wang, B., 1995: Interdecadal changes in El Niño onset in the last four decades. *J. Climate*, **8**, 267–285, doi: 10.1175/1520-0442(1995)008<0267:ICIENO>2.0.CO;2.

Wang, B., and Q. Zhang, 2002: Pacific-East Asian teleconnection. Part II: How the Philippine Sea anomalous anticyclone is established during El Niño development. *J. Climate*, **15**, 3252–3265, doi: 10.1175/1520-0442(2002)015<3252:PEATPI>2.

0.CO;2.

Wang, B., R. G. Wu, and X. H. Fu, 2000: Pacific-east Asian teleconnection: How does ENSO affect east Asian climate? *J. Climate*, **13**, 1517–1536, doi: 10.1175/1520-0442(2000)013<1517:PEATHD>2.0.CO;2.

Wang, B., R. G. Wu, and T. Li, 2003: Atmosphere-warm ocean interaction and its impacts on Asian-Australian monsoon variation. *J. Climate*, **16**, 1195–1211, doi: 10.1175/1520-0442(2003)16<1195:AOIAII>2.0.CO;2.

Wang, B., I.-S. Kang, and J.-Y. Lee, 2004: Ensemble simulations of Asian-Australian monsoon variability by 11 AGCMs. *J. Climate*, **17**, 803–818, doi: 10.1175/1520-0442(2004)017<0803:ESOAMV>2.0.CO;2.

Wang, B., Q. H. Ding, X. H. Fu, I.-S. Kang, K. Jin, J. Shukla, and F. Doblas-Reyes, 2005: Fundamental challenge in simulation and prediction of summer monsoon rainfall. *Geophys. Res. Lett*., **32**, L15711, doi: 10.1029/2005GL022734.

Wang, B., J. Liu, J. Yang, T. J. Zhou, and Z. W. Wu, 2009a: Distinct principal modes of early and late summer rainfall anomalies in East Asia. *J. Climate*, **22**, 3864–3875, doi: 10.1175/2009JCLI2850.1.

Wang, B., and Coauthors, 2009b: Advance and prospectus of seasonal prediction: assessment of the APCC/CliPAS 14-model ensemble retrospective seasonal prediction (1980-2004). *Climate Dyn*., **33**, 93–117, doi: 10.1007/s00382-008-0460-0.

Wang, B., B. Q. Xiang, and J.-Y. Lee, 2013: Subtropical high predictability establishes a promising way for monsoon and tropical storm predictions. *Proceedings of the National Academy of Sciences of the United States of America*, **110**, 2718–2722, doi: 10.1073/pnas.1214626110.

Wang, S. W., and Z. C. Zhao, 1981: Droughts and floods in China, 1470–1979. *Climate and History*, T. N. L. Wigley et al., Eds., Cambridge University Press, 271–288.

Wang, W.-C., and K. R. Li, 1990: Precipitation fluctuation over semiarid region in Northern China and the relationship with El Niño/Southern Oscillation. *J. Climate*, **3**, 769–783, doi: 10.1175/1520-0442(1990)003<0769:PFOSRI>2.0.CO;2.

Webster, P. J., A. M. Moore, J. P. Loschnigg, and R. R. Leben, 1999: Coupled ocean-atmosphere dynamics in the Indian Ocean during 1997–98. *Nature*, **401**, 356–360, doi: 10.1038/43848.

Wu, B., T. J. Zhou, and T. Li, 2009: Seasonally evolving dominant interannual variability modes of East Asian Climate. *J. Climate*, **22**, 2992–3005, doi: 10.1175/2008JCLI2710.1.

Wu, R. G., 2017: Relationship between Indian and East Asian summer rainfall variations. *Adv. Atmos. Sci*., **34**, 4–15, doi: 10.1007/ s00376-016-6216-6.

Wu, R. G., Z.-Z. Hu, and B. P. Kirtman, 2003: Evolution of ENSO-related rainfall anomalies in East Asia. *J. Climate*, **16**, 3742–3758, doi: 10.1175/1520-0442(2003)016<3742:EOERAI>2.0.CO;2.

Xiang, B. Q., B. Wang, W. D. Yu, and S. B. Xu, 2013: How can anomalous western North Pacific Subtropical High intensify in late summer? *Geophys. Res. Lett*., **40**, 2349–2354, doi: 10.1002/grl.50431.

Xie, S.-P., K. M. Hu, J. Hafner, H. Tokinaga, Y. Du, G. Huang, and T. Sampe, 2009: Indian ocean capacitor effect on Indo-Western Pacific climate during the summer following El Niño. *J. Climate*, **22**, 730–747, doi: 10.1175/2008JCLI2544.1.

Xie, S.-P., Y. Kosaka, Y. Du, K. M. Hu, J. S. Chowdary, and G. Huang, 2016: Indo-Western Pacific Ocean capacitor and coherent climate anomalies in Post-ENSO summer: A review. *Adv. Atmos. Sci*., **33**, 411–432, doi: 10.1007/s00376-015-5192-6.

Xing, W., B. Wang, and S.-Y. Yim, 2016: Peak-summer East Asian rainfall predictability and prediction part I: Southeast Asia. *Climate Dyn*., **47**, 1–13, doi: 10.1007/s00382-014-2385-0.

Xing, W., B. Wang, S.-Y. Yim, and K.-J. Ha, 2017: Predictable patterns of the May-June rainfall anomaly over East Asia. *J. Geophys. Res*., **122**, 2203–2217, doi: 10.1002/2016JD025856.

Yang, J. L., Q. Y. Liu, S.-P. Xie, Z. Y. Liu, and L. X. Wu, 2007: Impact of the Indian Ocean SST basin mode on the Asian summer monsoon. *Geophys. Res. Lett*., **34**, L02708, doi: 10.1029/2006GL028571.

Yasunari, T., 1991: The monsoon year-a new concept of the climatic year in the tropics. *Bull. Amer. Meteor. Soc*., **72**, 1331–1338, doi: 10.1175/1520-0477(1991)072<1331:TMYNCO>2.0.CO;2.

Yim, S.-Y., B. Wang, and M. Kwon, 2014a: Interdecadal change of the controlling mechanisms for East Asian early summer rainfall variation around the mid-1990s. *Climate Dyn*., **42**, 1325–1333, doi: 10.1007/s00382-013-1760-6.

Yim, S.-Y., B. Wang, and W. Xing, 2014b: Prediction of early summer rainfall over South China by a physical-empirical model. *Climate Dyn*., **43**, 1883–1891, doi: 10.1007/s00382-013-2014-3.

Yim, S.-Y., B. Wang, and W. Xing, 2016: Peak-summer East Asian rainfall predictability and prediction part II: Extratropical East Asia. *Climate Dyn*., **47**, 15–30, doi: 10.1007/s00382-015-2849-x.

Yuan, Y., and S. Yang, 2012: Impacts of different types of El Niño on the East Asian climate: Focus on ENSO cycles. *J. Climate*, **25**, 7702–7722, doi: 10.1175/JCLI-D-11-00576.1.

Zhang, R. H., A. Sumi, and M. Kimoto, 1999: A diagnostic study of the impact of El Niño on the precipitation in China. *Adv. Atmos. Sci*., **16**, 229–241, doi: 10.1007/BF02973084.